Comptes Rendus

Mécanique

Marwa Bouslema, Taher Fakhfakh, Rachid Nasri and Mohamed Haddar

Effect of elastic couplings on the dynamic behavior of transmission systems

Synthesis / *Synthèse*

Effect of elastic couplings on the dynamic behavior of transmission systems

Marwa Bouslema [*], [a, b], **Taher Fakhfakh** [a], **Rachid Nasri** [b]
and Mohamed Haddar [a]

[a] Mechanical Modeling and Manufacturing Laboratory (LA2MP), National School of
Engineers of Sfax, University of Sfax, B.P 1173-3038, Sfax, Tunisia

[b] Applied Mechanics and Engineering, University of El-Manar II, 1002 Tunis, Tunisia

E-mails: bouslema.marwa90@gmail.com (M. Bouslema), tahar.fakhfakh@gmail.com
(T. Fakhfakh), rachid.nasri@enit.rnu.tn (R. Nasri), mohamed.haddar@enis.rnu.tn
(M. Haddar)

Abstract. The aim of the present work is to analyze the sensibility of an elastic coupling on the coupled
Frequency Response Functions (FRFs) of transmission mechanical systems. The FRF of a linked system,
such as a reducer stage, is determined by a receptance coupling (RC) method. The equilibrium and the
compatibility conditions are applied.

   This method is investigated for different coupling models such as rigid and flexible. The proposed method
is validated by a direct computation of the full system showing exact agreement.

   Afterward, the effect of a rigid and a joined system on the sub-structuring response FRFs is analyzed.
The coupling models derived from literature review are discussed to show their effects on FRF. Although the
coupling in question is considered to be a flexible interface in the aforementioned system, as revealed in the
literature review, it introduces a translational and rotational damping and stiffness. So, the formulation of the
RC is different from the standard approach. In order to achieve the aim of the present work, the effects of some
important parameters such as translational and rotational coupling, shaft and bearing stiffness on the FRF
are discussed. Some sensitivity of the proposed models are observed in relation to the coupling parameters.

Keywords. Receptance coupling method, Elastic coupling, Frequency Response Functions (FRFs), Torsional
coupling stiffness, Translational coupling stiffness, Coupled system.

Manuscript received 21 June 2021, revised and accepted 8 June 2022.

1. Introduction

Complex systems are composed of several subsystems connected by means of an interface to
construct the assembled systems.

   Interfaces can have a great effect on the overall assembly compartment, such as natural
frequencies, mode shapes, and response characteristics. The mechanical properties and the
flexibility and damping at the interface level affect the coupled systems response [1]. As a

---

[*] Corresponding author.

consequence, it is cardinal to utilize coupling dynamic properties for the estimation of the overall assembled behavior system [2].

Many studies have set up diverse methods for investigation of coupling complex systems. The receptance coupling (RC) method is used to couple subsystems with a joint component based on the Frequency Response Functions (FRFs) in the machine tools application [3, 4]. This approach was suggested by Renand Beards [5] and Ewins [6] to characterize the interface properties. The influence of the joint parameters, modeled by a nonlinear spring, on coupling method was analyzed in [7]. The novel RC technique proposed by [8] required the FRF matrices of all subsystems comprising translational and rotational FRFs. Both methods of receptance can yield the coupled responses by discovering the distinction among the coupled system responses with rigid and flexible interfaces [9].

Liu *et al.* [6] selected the substructure method for the determination of dynamic properties of joints between coupled subsystems using FRFs. Recently, the singularity issue was implemented by El Mahmoudi *et al.* [10] while considering the flexible connection by means of substructures inside the (LM-FBS) coupling procedure. In addition, Tsai [11] tackled the problem of frequency assignment through coupling of subsystems using the receptance method.

Coupling plays an important role in turning machines in such a way that it couples the rotating parts. However, the presence of such mechanism without adding elastic parts can produce excessive vibration and noise. In order to mitigate such vibration, introducing elastic elements can be critical in that the natural frequencies would be away from the critical speed of the machines.

Recently, Wang *et al.* [12] examined the effects of different elastic support parameters on the dynamic behaviors of the wind turbine drive train using the FRFs. In addition, Bouaziz *et al.* [13] considered the flexible coupling to take the misalignment defect between rotating shafts. Tadeo and Cavla [14] investigated a system constituted of both flexible rotating shafts associated through a flexible coupling and assisted by hydrodynamic bearings to examine the impact of different linkers on the system response and notably the natural frequencies through the finite element method. The flexible coupling is investigated using distinct models. In the first model, the coupling was treated like a rigid disc. In the second model, the latter is constructed on Kramer's [15] initial approach through a coupling composed of both nodes presented with masses that regard the inertia effects. A third model is based on Kramer's [15] second approach that considered the rotational stiffness as well as damping. A fourth approach based on Nelson and Crandall's [16] first model is adopted to consider the coupling inertia including translational and rotational stiffness. The influence of three models of flexible coupling on the system response was studied by Chaika and Mariunas [17] for an electromechanical drive. So, it is important to carry out the modal analysis of gearbox and to study the effect of an elastic coupling use on the modal properties and therefore on the acoustic behavior of gearbox. The increase in bearing stiffness affects the rotor system properties [18]. Therefore, the necessity to analyse the gearbox model and to characterize the influence of elastic coupling on the FRF is the focus of this work.

The main goal of the suggested approach is to prove the effect of the interface by comparing the FRFs of a rigid and a joined system of identical dimensions. The effects of the shafts, bearing and coupling stiffness are analyzed on the system response.

The development of a RC method for the different joints are treated in Section 2. The dynamic model of a reducer stage system are described in Section 3.

The double reducer stage is considered to analyse the model properties in both cases with rigid and elastic coupling. Results obtained with rigid coupling are compared with those obtained by flexible coupling, employing the second approach of Kramer [15] and Nelson [16]. The variance among the responses of the assembled system linked with rigid and flexible joints are discussed in Section 4.
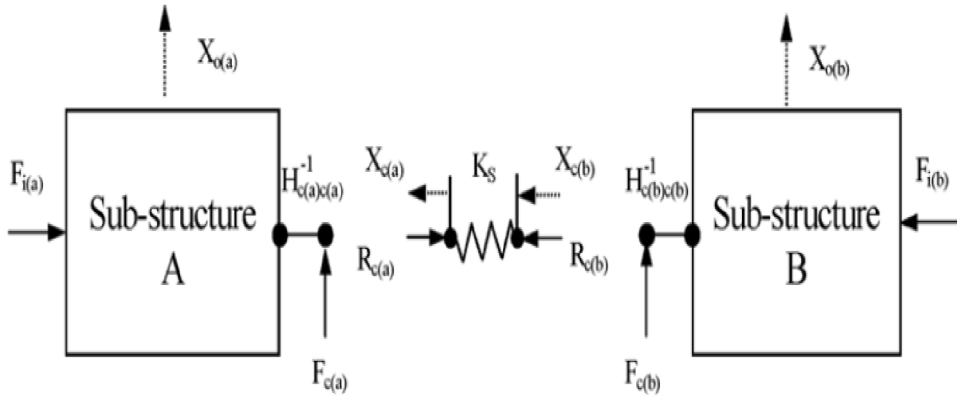
Figure 1. Flexible connector system of two subsystems [19].

2. Theoretical formulation

The RC technique determined the dynamic behavior of a coupled system based on the uncoupled subsystems' FRFs.

In this section, the two RC techniques are described. The FRFs of each subsystem and their coupling are determined.

2.1. *Frequency Response Functions coupling with rigid and flexible joint*

A major mechanical system generally includes many subsystems. For simplicity, the assembled system is divided into two subsystems, as displayed in Figure 1. The interface can be modeled like linear spring ks, as presented in Figure 1.

Free subsystems can be represented by receptance matrices. Their expressions are presented in [20].

The available degrees of freedom (DoFs) for each uncoupled subsystem are divided into internal DoFs i for subsystem A and j for subsystem B and coupling DoFs denoted c. The subsystem A is connected to subsystem B by a flexible coupling at DoFs c. The coupling method imposes compatibility and equilibrium conditions at the interface as presented by Jetmundsen *et al.* [21]. This idea is applied to the frequency-based substructuring (FBS) equation for both rigid and flexible coupling. The FRFs of the coupling DoFs between two subsystems A and B were expressed as in [22]:

$$
\begin{aligned}
AB[\boldsymbol{H}] &= \begin{bmatrix} [\boldsymbol{H}]_{aa} & [\boldsymbol{H}]_{ac} & [\boldsymbol{H}]_{ab} \\ [\boldsymbol{H}]_{ca} & [\boldsymbol{H}]_{cc} & [\boldsymbol{H}]_{cb} \\ [\boldsymbol{H}]_{ba} & [\boldsymbol{H}]_{bc} & [\boldsymbol{H}]_{bb} \end{bmatrix} \\
&= \begin{bmatrix} {}_A[\boldsymbol{H}]_{ii} & {}_A[\boldsymbol{H}]_{ic} & \mathbf{0} \\ {}_A[\boldsymbol{H}]_{ci} & {}_A[\boldsymbol{H}]_{cc} & \mathbf{0} \\ \mathbf{0} & \mathbf{0} & {}_B[\boldsymbol{H}]_{jj} \end{bmatrix} - \begin{bmatrix} {}_A[\boldsymbol{H}]_{ic} \\ {}_A[\boldsymbol{H}]_{cc} \\ {}_B[\boldsymbol{H}]_{jc} \end{bmatrix} ({}_A[\boldsymbol{H}]_{cc} + {}_B[\boldsymbol{H}]_{cc} + [\boldsymbol{K}]_s^{-1})^{-1} \begin{bmatrix} {}_A[\boldsymbol{H}]_{ic} \\ {}_A[\boldsymbol{H}]_{cc} \\ {}_B[\boldsymbol{H}]_{jc} \end{bmatrix}^T,
\end{aligned} \quad (1)
$$

where ${}_{AB}[\boldsymbol{H}]$ denotes the assembled system matrix. $[\boldsymbol{K}_s]$ represents the coupling stiffness matrix between the coupling DoFs of both subsystems. ${}_A[\boldsymbol{H}]_{cc}$, ${}_B[\boldsymbol{H}]_{cc}$ and $[\boldsymbol{K}]_s^{-1}$ are the diagonal elements. The global system coupling FRF is calculated using (1). For a rigid joint, the Kernel matrix $({}_A[\boldsymbol{H}]_{cc} + {}_B[\boldsymbol{H}]_{cc} + [\boldsymbol{K}]_s^{-1})$ in (1) is substituted by $({}_A[\boldsymbol{H}]_{cc} + {}_B[\boldsymbol{H}]_{cc})^{-1}$ [23]. In this formulation, the cross-coupled properties of the interface between the translational (TDoF) and the rotational (RDOF) are neglected.

2.2. *Receptance coupling method*

In the RC method, the analytical or experimental subsystems FRFs are mathematically linked to access the assembled system response. The connection between subsystems A and B through the interface is shown in Figure 1. The indices $c1$ and $c2$ illustrate the DOFs of the joint interface. Including interface dynamics, the formulated receptance matrices of each subsystems are presented as [8]:

$$\begin{Bmatrix} A[\boldsymbol{x}]_i \\ A[\boldsymbol{\theta}]_i \\ A[\boldsymbol{x}]_c \\ A[\boldsymbol{\theta}]_c \end{Bmatrix} = \begin{bmatrix} A[\boldsymbol{S}]_{ii} & A[\boldsymbol{L}]_{ii} & A[\boldsymbol{S}]_{ic} & A[\boldsymbol{L}]_{ic} \\ A[\boldsymbol{N}]_{ii} & A[\boldsymbol{P}]_{ii} & A[\boldsymbol{N}]_{ic} & A[\boldsymbol{P}]_{ic} \\ A[\boldsymbol{S}]_{ci} & A[\boldsymbol{L}]_{ci} & A[\boldsymbol{S}]_{cc} & A[\boldsymbol{L}]_{cc} \\ A[\boldsymbol{N}]_{ci} & A[\boldsymbol{P}]_{ci} & A[\boldsymbol{N}]_{cc} & A[\boldsymbol{P}]_{cc} \end{bmatrix} \begin{Bmatrix} A[\boldsymbol{f}]_i \\ A[\boldsymbol{M}]_i \\ A[\boldsymbol{f}]_c + A[\boldsymbol{f}]_{c1} \\ A[\boldsymbol{M}]_c + A[\boldsymbol{M}]_{c1} \end{Bmatrix},$$

$$\begin{Bmatrix} B[\boldsymbol{x}]_j \\ B[\boldsymbol{\theta}]_j \\ B[\boldsymbol{x}]_c \\ B[\boldsymbol{\theta}]_c \end{Bmatrix} = \begin{bmatrix} B[\boldsymbol{S}]_{jj} & B[\boldsymbol{L}]_{jj} & B[\boldsymbol{S}]_{jc} & B[\boldsymbol{L}]_{jc} \\ B[\boldsymbol{N}]_{jj} & B[\boldsymbol{P}]_{jj} & B[\boldsymbol{N}]_{jc} & B[\boldsymbol{P}]_{jc} \\ B[\boldsymbol{S}]_{cj} & B[\boldsymbol{L}]_{cj} & B[\boldsymbol{S}]_{cc} & B[\boldsymbol{L}]_{cc} \\ B[\boldsymbol{N}]_{cj} & B[\boldsymbol{P}]_{cj} & B[\boldsymbol{N}]_{cc} & B[\boldsymbol{P}]_{cc} \end{bmatrix} \begin{Bmatrix} B[\boldsymbol{f}]_j \\ B[\boldsymbol{M}]_j \\ B[\boldsymbol{f}]_c + B[\boldsymbol{f}]_{c2} \\ B[\boldsymbol{M}]_c + B[\boldsymbol{M}]_{c2} \end{Bmatrix}, \tag{2}$$

where $A[\boldsymbol{x}]_i$ and $A[\boldsymbol{\theta}]_i$ (resp $B[\boldsymbol{x}]_j$ and $B[\boldsymbol{\theta}]_j$) indicate the translational and rotational displacement vectors. The receptance components too are determined as $\boldsymbol{S} = \boldsymbol{x}/\boldsymbol{f}$, $\boldsymbol{L} = \boldsymbol{x}/\boldsymbol{M}$, $\boldsymbol{N} = \boldsymbol{\theta}/\boldsymbol{f}$ and $\boldsymbol{P} = \boldsymbol{\theta}/\boldsymbol{M}$. The stiffness and damping were considered in the interface parameters. The equilibrium and compatibility conditions at the interface are:

$$\begin{Bmatrix} A[\boldsymbol{f}]_{c1} \\ A[\boldsymbol{f}]_{c1} \\ A[\boldsymbol{M}]_{c1} \end{Bmatrix} + \begin{Bmatrix} B[\boldsymbol{f}]_{c2} \\ B[\boldsymbol{f}]_{c2} \\ B[\boldsymbol{M}]_{c2} \end{Bmatrix} = \{\boldsymbol{0}\}. \tag{3}$$

Using the equilibrium conditions, the equations of motion at the joint part can be written as

$$c_x({}_B\dot{x}_c - {}_A\dot{x}_c) + k_x({}_Bx_c - {}_Ax_c) = {}_A\boldsymbol{f}_{c1} \tag{4}$$

$$c_y({}_B\dot{y}_c - {}_A\dot{y}_c) + k_y({}_By_c - {}_Ay_c) = {}_A\boldsymbol{f}_{c1} \tag{5}$$

$$c_\theta({}_B\dot{\theta}_c - {}_A\dot{\theta}_c) + k_\theta({}_B\theta_c - {}_A\theta_c) = {}_A\boldsymbol{M}_{c1}, \tag{6}$$

where k_x, k_θ (resp. c_x, c_θ) are the translational and rotational stiffness (resp. damping) of the joint. Applying the Laplace transformation to (4)–(6) and replacing s by iw, Equations (4)–(6) can be rewritten in the frequency domain as:

$$\begin{Bmatrix} {}_Bx_c - {}_Ax_c \\ {}_By_c - {}_Ay_c \\ {}_B\theta_c - {}_A\theta_c \end{Bmatrix} = [H_j] \begin{Bmatrix} {}_A\boldsymbol{f}_{c1} \\ {}_A\boldsymbol{f}_{c1} \\ {}_A\boldsymbol{M}_{c1} \end{Bmatrix}, \tag{7}$$

where $[H_j]$ denotes the receptance matrix of the joint expressed as:

$$[H_j] = \begin{bmatrix} h_{tt} & 0 & 0 \\ 0 & h_{tt} & 0 \\ 0 & 0 & h_{rr} \end{bmatrix}, \tag{8}$$

where subscripts t and r represent the two translational and rotational directions, respectively. Substituting (2) and (3) leads to the assembled system FRFs as

$$\begin{Bmatrix} A[\boldsymbol{f}]_{c1} \\ A[\boldsymbol{M}]_{c1} \end{Bmatrix} = -\begin{Bmatrix} B[\boldsymbol{f}]_{c2} \\ B[\boldsymbol{M}]_{c2} \end{Bmatrix} = -B^{-1}H_{c1i}\begin{Bmatrix} B[\boldsymbol{f}]_i \\ B[\boldsymbol{M}]_i \end{Bmatrix} - B^{-1}H_{c1c1}\begin{Bmatrix} B[\boldsymbol{f}]_{c1} \\ B[\boldsymbol{M}]_{c1} \end{Bmatrix} + B^{-1}H_{c2c2}\begin{Bmatrix} B[\boldsymbol{f}]_{c2} \\ B[\boldsymbol{M}]_{c2} \end{Bmatrix}$$

$$+ B^{-1}H_{c2j}\begin{Bmatrix} B[\boldsymbol{f}]_j \\ B[\boldsymbol{M}]_j \end{Bmatrix}, \tag{9}$$

where $B = {}_AH_{cc} + {}_BH_{cc} + [H_{ij}]$ and $[H_{ij}] = [S_{ij}L_{ij}; N_{ij}P_{ij}]$. Substituting (2) and (9) leads to the assembled system FRFs as:

$$
\begin{Bmatrix} {}_s[\textbf{X}]_i \\ {}_s[\textbf{X}]_j \\ {}_s[\textbf{X}]_{c1} \\ {}_s[\textbf{X}]_{c2} \end{Bmatrix} = \begin{bmatrix} {}_s[\textbf{G}]_{ii} & {}_s[\textbf{G}]_{ic1} & {}_s[\textbf{G}]_{ic2} & {}_s[\textbf{G}]_{ij} \\ {}_s[\textbf{G}]_{c1i} & {}_s[\textbf{G}]_{c1c1} & {}_s[\textbf{G}]_{c1c2} & {}_s[\textbf{G}]_{c1j} \\ {}_A[\textbf{G}]_{c2i} & {}_A[\textbf{G}]_{c2c2} & {}_s[\textbf{G}]_{c2c1} & {}_s[\textbf{G}]_{c2j} \\ {}_s[\textbf{G}]_{ji} & {}_s[\textbf{G}]_{jc1} & {}_s[\textbf{G}]_{jc2} & {}_s[\textbf{G}]_{jj} \end{bmatrix} \begin{Bmatrix} {}_A[\textbf{F}]_i \\ {}_A[\textbf{F}]_i \\ {}_A[\textbf{F}]_{c1} \\ {}_A[\textbf{F}]_{c2} \end{Bmatrix},
\tag{10}
$$

where $[G_{ij}] = [G_{ij,tt}G_{ij,tr}; G_{ij,rt}G_{ij,rr}]$ represents the assembled system and $X_i = x_i\theta_i$ is the displacement vector of the linked system. The coupled response at positions 1 and 2 can be expanded as [8]:

$$
\begin{bmatrix} \textbf{G}_{ii,tt} & \textbf{G}_{ii,tr} \\ \textbf{G}_{ii,rt} & \textbf{G}_{ii,rr} \end{bmatrix} = \begin{bmatrix} \textbf{S}_{ii} & \textbf{L}_{ii} \\ \textbf{N}_{ii} & \textbf{P}_{ii} \end{bmatrix} - \begin{bmatrix} \textbf{S}_{ic1} & \textbf{L}_{ic1} \\ \textbf{N}_{ic1} & \textbf{P}_{ic1} \end{bmatrix} \begin{bmatrix} \textbf{b}_{tt} & \textbf{b}_{tr} \\ \textbf{b}_{rt} & \textbf{b}_{rr} \end{bmatrix}^{-1} \begin{bmatrix} \textbf{S}_{c1i} & \textbf{L}_{c1i} \\ \textbf{N}_{c1i} & \textbf{P}_{c1i} \end{bmatrix},
\tag{11}
$$

where

$$
\begin{bmatrix} \textbf{b}_{tt} & \textbf{b}_{tr} \\ \textbf{b}_{rt} & \textbf{b}_{rr} \end{bmatrix} = \begin{bmatrix} \textbf{S}_{c1c1} & \textbf{L}_{c1c1} \\ \textbf{N}_{c1c1} & \textbf{P}_{c1c1} \end{bmatrix} + \begin{bmatrix} \textbf{S}_{c2c2} & \textbf{L}_{c2c2} \\ \textbf{N}_{c2c2} & \textbf{P}_{c2c2} \end{bmatrix} + \begin{bmatrix} \textbf{H}_{tt} & 0 \\ 0 & \textbf{H}_{rr} \end{bmatrix}.
\tag{12}
$$

These two FRFs are expanded as

$$\textbf{G}_{ii,tt} = xii/fii = \textbf{S}_{ii} - (1/(\textbf{b}_{tt}\textbf{b}_{rr} - \textbf{b}_{rt}\textbf{b}_{tr}))[(\textbf{S}_{ic1}\textbf{b}_{rr} - \textbf{L}_{ic1}\textbf{b}_{rt})\textbf{S}_{c1i} + (-\textbf{S}_{c1i}\textbf{b}_{tr} + \textbf{L}_{ic1}\textbf{b}_{tt})\textbf{N}_{c1i}] \tag{13}$$

$$\textbf{G}_{ii,rr} = xii/Mii = \textbf{P}_{ii} - (1/(\textbf{b}_{tt}\textbf{b}_{rr} - \textbf{b}_{rt}\textbf{b}_{tr}))[(\textbf{P}_{ic1}\textbf{b}_{tt} - \textbf{N}_{c1i}\textbf{b}_{tr})\textbf{P}_{c1i} + (-\textbf{P}_{c1i}\textbf{b}_{rt} + \textbf{N}_{ic1}\textbf{b}_{rr})\textbf{P}_{c1i}] \tag{14}$$

$$\textbf{G}_{12,tt} = xii/fc1 = \textbf{S}_{ic1} - (1/(\textbf{b}_{tt}\textbf{b}_{rr} - \textbf{b}_{rt}\textbf{b}_{tr}))[(\textbf{S}_{ic1}\textbf{b}_{rr} - \textbf{L}_{ic1}\textbf{b}_{rt})\textbf{S}_{c2c2} + (-\textbf{S}_{c1i}\textbf{b}_{tr} + \textbf{L}_{ic1}\textbf{b}_{tt})\textbf{N}_{c2c2}] \tag{15}$$

$$\textbf{G}_{c2c2,tt} = xc2/Mc2 = \textbf{S}_{c2c2} - (1/(\textbf{b}_{tt}\textbf{b}_{rr} - \textbf{b}_{rt}\textbf{b}_{tr}))[(\textbf{S}_{ic1}\textbf{b}_{rr} - \textbf{L}_{ic1}b_{rt})\textbf{S}_{c2c2} + (-\textbf{S}_{c1i}\textbf{b}_{tr} + \textbf{L}_{ic1}\textbf{b}_{tt})\textbf{N}_{c2c2}]. \tag{16}$$

2.3. *Determination of the FRF*

The format of the motion equation in the frequency domain depends on the physical parameter used in the investigation. Typically the equation of motion is scripted in displacement, which takes it to:

$$\{\textbf{X}(\omega)\} = [\textbf{H}(\omega)]\{\textbf{F}(\omega)\}, \quad [\textbf{H}(\omega)]^{-1} = [\textbf{K}] - \omega^2[\textbf{M}] + j\omega[\textbf{C}]. \tag{17}$$

The FRF synthesis attributed to mode shapes and natural frequencies is used to determined the FRF of a mechanical system. The relationship between the FRF matrix $\textbf{H}_{jk}(\omega)$ and mode shapes is made explicit by:

$$\textbf{H}_{jk}(\omega) = \sum_{r=1}^{n} \frac{{}^r\Phi_j \, {}^r\Phi_k}{\omega_r^2 - \omega^2 + 2j\xi_r\omega_r\omega}, \tag{18}$$

where $\textbf{H}_{jk}(\omega)$ is the steady-state response. n denotes the DoFs. ${}^r\Phi_j$ is the mass-normalized eigenvector.

3. Numerical models

Figure 2 depicts the system of interest, composed of two reducer stage spur gear mechanisms connected through flexible coupling.

The coupling response on assembled system is studied by three dynamic models. In the first study, the joint is characterized by a rigid coupling. The first model considered here is the first model suggested by Krämer [15]. The coupling is modeled as a rigid disc, with equal parts at the coordinates connecting the coupling to the adjoining shafts corresponding to the coupling inertia. The second and the third study selects the identical reducer stages, coupled with flexible coupling. First, the elastic coupling is approximated via Krämer model [15] with torsional stiffness ($k_{\theta c}$) and torsional damping ($c_{\theta c}$)(shown in Figure 3(a)). Second, it is according to the model of Nelson and Crandall [16] with radial stiffness (k_{xc}, k_{yc}), torsional stiffness ($k_{\theta c}$), radial damping
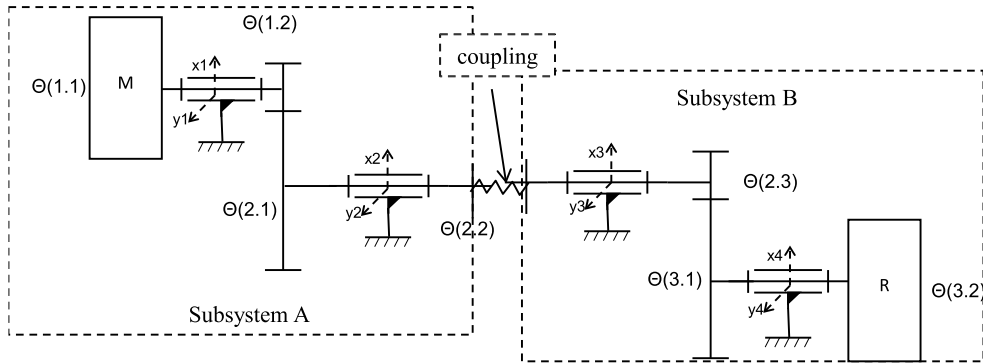
Figure 2. Kinematic scheme of reducer stage connected with flexible interface.
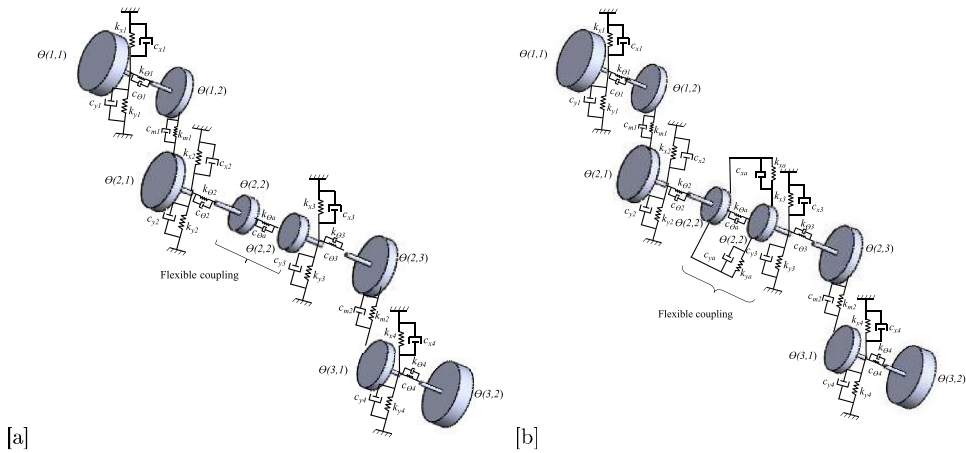
Figure 3. Lumped parameter of reducer stage connected with flexible interface.

(c_{xc}, c_{yc}) and torsional damping ($c_{\theta c}$) (shown Figure 3(b)). The two models contained the inertial effects as two inflexible disks (I_{22}) and (I_{23}).

The pinions and the gears are taken into consideration as rigid bodies for each stage and their inertia are respectively $I(1,2), I(2,1), I(2,3)$ and $I(3,1)$. The shafts are supposed to be massless with torsional stiffness $k_{\theta i}$ and torsional damping $c_{\theta i}$ ($i = 1,2,3,4$). The shafts are supported by radial stiffness of bearings modeled by parallel springs (k_{xj} and k_{yj}) and dampers (c_{xj} and c_{yj}). The two stages are modeled by constant meshing stiffness, respectively (1,2) with (2,1) and (2,3) with (3,1). The wheels (1,1) and (3,2) denote the motor and the receiver sides, respectively. The inertia of motor and receiver are presented by I_m and I_r, respectively. The shaft (2) is linked to the shaft (3) by the elastic interface. An interface model includes translational and torsional FRFs and considers the joint properties.

3.1. *Coupling method*

The aforementioned method involves dividing the full system into two subsystems as depicted in Figure 2. The coupling is divided into two equal parts as in [24]. The two subsystems can be analyzed separately, then the FRF is integrated on the full system. A modeling of the two-stage

spur gear transmission is proposed in [25]. The motion equation of a damped linear system is expressed by:

$$[M]\{\ddot{X}(t)\} + [C]\{\dot{X}(t)\} + [K]\{X(t)\,t\} = \{F(t)\}. \tag{19}$$

To determine the mass [M], damping [C] and stiffness [K] of each subsystem, we use (19). The stiffness matrix [K] is expressed as:

$$[K] = [K_s] + [K(t)], \tag{20}$$

where K_s presents the stationary stiffness matrix of bearing and shaft, $K(t)$ the time-varying mesh stiffness matrix. [$K(t)$] can be divided into an average stiffness matrix [k_m] and a time-variable stiffness matrix [$k(t)$]. We supposed a constant gear stiffness and neglected the variable stiffness.

The generalized coordinate vector of the linear dynamic model X includes eight DoFs and can be defined by:

$$X = [X_1\ X_c]^T, \quad X_1 = \begin{bmatrix} x_1\ y_1\ x_2\ y_2\ \theta(1,1)\ \theta(1,2)\ \theta(2,1) \end{bmatrix}^T, \quad X_c = [\theta(2,2)]^T. \tag{21}$$

These DoFs can be distributed into internal and coupling DoFs X_1 and X_c, respectively. The generalized coordinate vector of the linear dynamic model X for the second RC method includes eight DoFs which can be defined by:

$$X = [X_1\ X_c]^T, \quad X_1 = \begin{bmatrix} x_1\ y_1\ \theta(1,1)\ \theta(1,2)\ \theta(2,1) \end{bmatrix}^T, \quad X_c = \begin{bmatrix} x_2\ y_2\ \theta(2,2) \end{bmatrix}. \tag{22}$$

The two mass matrices [M] and [M'] are expressed by:

$$[M] = \mathrm{diag}[m(1,1), m(1,1), m(2,1), m(2,1), I(1,1), I(1,2), I(2,1), I(2,2)/2], \tag{23}$$

$$[M'] = \mathrm{diag}[m(1,1), m(1,1), I(1,1), I(1,2), I(2,1), m(2,1), m(2,1), I(2,2)/2], \tag{24}$$

where $m(i,1)$ are the mass of wheels and pinions ($i = 1,2$). $I(1,1)$, $I(1,2)$, $I(2,1)$ and $I(2,2)$ are the motor inertia, the wheels inertia, the pinions inertia and the coupling inertia, respectively.

The stiffness and the damping matrices [K] and [C] are composed of the bearing stiffness and damping k_{xi}, k_{yi} and c_{xi}, c_{yi}, where ($i = 1,2$). The torsional stiffness and damping are $k_{\theta i}$ and $c_{\theta i}$, where ($i = 1,2$). The gear mesh stiffness and damping, denoted by [k_m] and [c_m], are expressed as [26]:

$$[K] = \begin{bmatrix}
s_3 k_m + k_{x1} & s_5 k_m & -s_3 k_m & -s_5 k_m & 0 & s_7 k_m & s_9 k_m & 0 \\
s_5 k_m & s_4 k_m + k_{y1} & -s_5 k_m & -s_4 k_m & 0 & s_6 k_m & s_8 k_m & 0 \\
-s_3 k_m & -s_5 k_m & s_3 k_m + k_{x2} & s_5 k_m & 0 & -s_7 k_m & -s_9 k_m & 0 \\
s_5 k_m & -s_4 k_m & s_5 k_m & s_4 k_m + k_{y2} & 0 & -s_6 k_m & s_8 k_m & 0 \\
0 & 0 & 0 & 0 & k_{\theta 1} & -k_{\theta 1} & 0 & 0 \\
s_7 k_m & s_6 k_m & -s_7 k_m & -s_6 k_m & -k_{\theta 1} & s_{10} k_m + k_{\theta 1} & s_{12} k_m & 0 \\
s_9 k_m & s_8 k_m & -s_9 k_m & s_9 k_m & 0 & s_{12} k_m & s_{11} k_m + k_{\theta 2} & -k_{\theta 2} \\
0 & 0 & 0 & 0 & 0 & 0 & -k_{\theta 2} & k_{\theta 2}
\end{bmatrix}, \tag{25}$$

$$[C] = \begin{bmatrix}
s_3 c_m + c_{x1} & s_5 c_m & -s_3 c_m & -s_5 c_m & 0 & s_7 c_m & s_9 c_m & 0 \\
s_5 c_m & s_4 c_m + c_{y1} & -s_5 c_m & -s_4 c_m & 0 & s_6 c_m & s_8 c_m & 0 \\
-s_3 c_m & -s_5 c_m & s_3 c_m + c_{x2} & s_5 c_m & 0 & -s_7 c_m & -s_9 c_m & 0 \\
s_5 c_m & -s_4 c_m & s_5 c_m & s_4 c_m + c_{y2} & 0 & -s_6 c_m & s_8 c_m & 0 \\
0 & 0 & 0 & 0 & c_{\theta 1} & -c_{\theta 1} & 0 & 0 \\
s_7 c_m & s_6 c_m & -s_7 c_m & -s_6 c_m & -c_{\theta 1} & s_{10} c_m + c_{\theta 1} & s_{12} c_m & 0 \\
s_9 c_m & s_8 c_m & -s_9 c_m & s_9 c_m & 0 & s_{12} c_m & s_{11} c_m + c_{\theta 2} & -c_{\theta 2} \\
0 & 0 & 0 & 0 & 0 & 0 & -c_{\theta 2} & c_{\theta 2}
\end{bmatrix}. \tag{26}$$

The stiffness and the damping matrices $[K']$ and $[C']$ are expressed in the second receptance method by:

$$[K'] = \begin{bmatrix} s_3 k_m + k_{x1} & s_5 k_m & 0 & s_7 k_m & s_9 k_m & -s_3 k_m & -s_5 k_m & 0 \\ s_5 k_m & s_4 k_m + k_{y1} & 0 & s_6 k_m & s_8 k_m & -s_5 k_m & -s_4 k_m & 0 \\ 0 & 0 & k_{\theta 1} & -k_{\theta 1} & 0 & 0 & 0 & 0 \\ s_7 k_m & s_6 k_m & -k_{\theta 1} & s_{10} k_m + k_{\theta 1} & s_{12} k_m & -s_7 k_m & -s_6 k_m & 0 \\ s_9 k_m & s_8 k_m & 0 & s_{12} k_m & s_{11} k_m + k_{\theta 2} & -s_9 k_m & s_9 k_m & -k_{\theta 2} \\ -s_3 k_m & -s_5 k_m & 0 & -s_7 k_m & -s_9 k_m & s_3 k_m + k_{x2} & s_5 k_m & 0 \\ s_5 k_m & -s_4 k_m & 0 & -s_6 k_m & s_8 k_m & s_5 k_m & s_4 k_m + k_{y2} & 0 \\ 0 & 0 & 0 & 0 & -k_{\theta 2} & 0 & 0 & k_{\theta 2} \end{bmatrix}, \quad (27)$$

$$[C'] = \begin{bmatrix} s_3 c_m + c_{x1} & s_5 c_m & 0 & s_7 c_m & s_9 c_m & -s_3 c_m & -s_5 c_m & 0 \\ s_5 c_m & s_4 c_m + c_{y1} & 0 & s_6 c_m & s_8 c_m & -s_5 c_m & -s_4 c_m & 0 \\ 0 & 0 & c_{\theta 1} & -c_{\theta 1} & 0 & 0 & 0 & 0 \\ s_7 c_m & s_6 c_m & -c_{\theta 1} & s_{10} c_m + c_{\theta 1} & s_{12} c_m & -s_7 c_m & -s_6 c_m & 0 \\ s_9 c_m & s_8 c_m & 0 & s_{12} c_m & s_{11} c_m + c_{\theta 2} & -s_9 c_m & s_9 c_m & -c_{\theta 2} \\ -s_3 c_m & -s_5 c_m & 0 & -s_7 c_m & -s_9 c_m & s_3 c_m + c_{x2} & s_5 c_m & 0 \\ s_5 c_m & -s_4 c_m & 0 & -s_6 c_m & s_8 c_m & s_5 c_m & s_4 c_m + c_{y2} & 0 \\ 0 & 0 & 0 & 0 & -c_{\theta 2} & 0 & 0 & c_{\theta 2} \end{bmatrix}, \quad (28)$$

where the variables s_i, $i = 1, 2, \ldots, 12$ are given by:

$$\begin{aligned} s_1 &= \sin \alpha, \quad s_2 = \cos \alpha, \quad s_3 = \sin \alpha, \quad s_4 = \cos \alpha, \quad s_5 = \sin \alpha \cos \alpha, \quad s_6 = r_{b12} \cos \alpha \\ s_7 &= r_{b12} \sin \alpha, \quad s_8 = r_{b21} \cos \alpha, \quad s_9 = r_{b21} \sin \alpha, \quad s_{10} = r_{b12}^2, \quad s_{11} = r_{b21}^2, \quad s_{12} = r_{b12} r_{b21}, \end{aligned} \quad (29)$$

where r_{b12}, r_{b21} are the base radius of the pinion and the gear, respectively.

4. Numerical simulations and discussions

The RC technique is applied using a flexible coupling between the two subsystems A and B. The first study discussed the effect of a flexible coupling on the coupled system FRF. Subsequently, a parametric study is applied to discuss the influence of the interface and the subsystem parameters' variation on system response.

4.1. *Validation of substructuring in flexible coupling*

The model of reducer stage with an elastic coupling using the approach of substructuring method is investigated. In the validation case, the elastic coupling is localized between the motor and the spur gearbox. Thus, the global system is divided on two subsystems A and B with two equal halves of the coupling inertia. The aforementioned model is investigated by comparing with the work suggested by Hmida *et al.* [27] and Chaarii [26] as a reference. For instance, Figure 4 depicts the FRF of a subsystem B with flexible coupling in the radial direction of the third bearing (y_3 direction). The displayed peaks conform to the natural frequencies of subsystem A, B and coupling. These peaks presented the rotation and the bending modes. The coupled frequency corresponds to 26 Hz as presented in the zoomed inset in the figure.

The natural frequencies of the gearbox obtained with the proposed dynamic substructuring method were compared to direct FRF results of Hmida *et al.* [27] which is presented in Table 1. An excellent agreement is observed, with error reaching 0.6%.

In fact, the numerical results show a good correlation of the noted natural frequencies through the same conditions and paramters of gearbox mentioned by Hmida *et al.* [27]. Also the same FRFs curves of the third bearing (y_3 direction) for two methods is shown in Figure 4. Therefore, the proposed method of FRF applied to gearbox is validated. Furthermore, the effectiveness of this method in reducing the computation time is proved in [20].
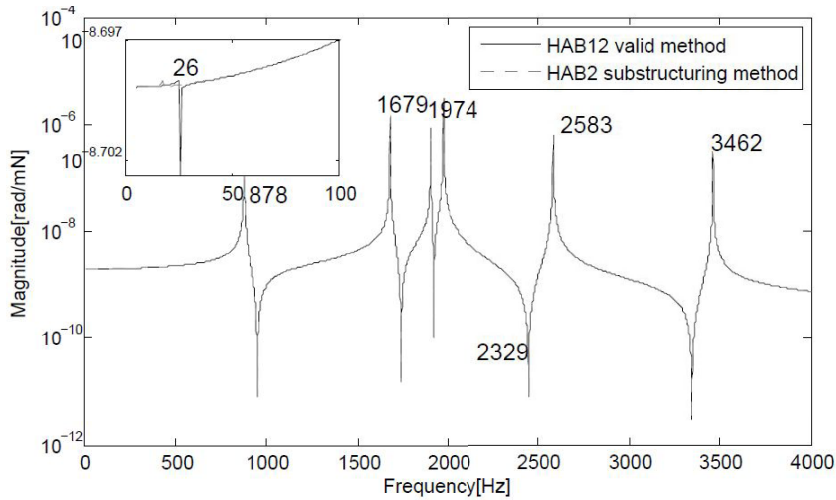
Figure 4. FRF in the linear direction of the third bearing with flexible coupling.

Table 1. Natural frequencies of present work and Hmida *et al.* [27] (2017)

Frequency system	Present work (Hz)	Hmida (2017) (Hz)
F1	18 (0.3%)	26
F2	875	878
F3	1583	1583.8
F4	1679	1679.6
F5	1902	1902.3
F6	1972	1972
F7	1974	1974.2
F8	1974	1974.2
F9	2329 (0.6%)	2344.4
F10	2583 (0.3%)	2591.1
F11	3462 (0.23%)	3470.3

4.2. *Results of flexible receptance coupling*

This work permits to discuss and collate the FRF of the connections models proposed via Krämer [15] and also the FRF of the coupling model as a rigid disk. The substructuring method is first applied to rigid coupling subsystems which is validated with the work done in [28]. The considered case describes two subsystems including the identical parameters through both stages of reducer. The values of the transmission and coupling parameters are given in Table 2.

The resolution of the eigenvalue problem is carried out for the determination of the frequencies subsystems and the overall system. To analyze the dynamic behavior of the coupled system, the eigenfrequencies of the two subsystems A and B and the global system (AB) are presented in Table 3.

The natural frequencies of the coupled system correspond to the eigenfrequencies of the individual subsystem and modified frequencies, classified as global (coupled) frequencies, which are 260, 630, 870 and 1910 Hz. The effect of a flexible coupling on the natural frequency values was investigated. Figures 5(a) and (b) depict the FRF of a subsystem A with rigid and flexible

Table 2. Parameters of the studied two-stage gear system

Mass of wheel and pinion (kg)	$m(1) = 2.66, m(2) = 6.04$
Inertia moment of wheel and pinion (kg·m^2)	$I(1) = 0.0048, I(2) = 0.0243$
Bearing stiffness (N/m)	$k_{xi} = k_{yi} = 10^8$
Bearing damping (N·s/m)	$c_{xi} = c_{yi} = 0.5$
Torsional damping (N·m·s/rad)	$c_{\theta i} = 5.5 \times 10^{-2}$
Torsional shaft flexibilities (N·m/rad)	$k_{\theta i} = 10^5$
Pressure angle	$\alpha_1 = \alpha_2 = 20°$
Teeth module (m)	$m = 4 \times 10^{-3}$
Teeth number	$Z_1 = 30; Z_2 = 45; Z_3 = 30; Z_4 = 45$
Average mesh stiffness (N/m)	$k_{1moy} = k_{2moy} = 8.4 \times 10^7$
Teeth width (m)	$b = 3 \times 10^{-2}$
Inertia coupling (kg·m^2)	$I(A) = 4.48 \times 10^{-8}; I(A) = 4 \times 10^{-4}$
Torsional stiffness of coupling (N·m/rad)	$k_{\theta i} = 2 \times 10^4$
Translational stiffness (N/m)	$k_{xa} = k_{ya} = 462 \times 10^2$

Table 3. Natural frequencies of two subsystems *A*, *B* and global system (*AB*) (Hz)

Subsystem *A*	Subsystem *B*	Global system (*AB*)
0	0	0
530	550	260
650	650	530
790	650	630
970	840	650
1110	970	650
1950	1880	650
33,628	33,628	790
–	–	870
–	–	970
–	–	970
–	–	1110
–	–	1910
–	–	1950
–	–	33,628

coupling in the radial direction of the second bearing (y_2 direction) and the torsional direction of the second shaft. Different stiffness values of coupling were taken in this study. The FRF curves obtained by a substructuring method are calculated via (1). The difference appearing in the frequency is due to the coupling torsional stiffness. Besides the torsional direction is sensible to the variation of the coupling torsional stiffness. So, the results show that the interface parameters decreased the coupling natural frequencies and the magnitude. The torsional frequency of the connection shaft appears at 5000 Hz. On the other hand, this frequency shift towards a high frequency in the case of a rigid coupling is because of the low inertia of the coupling. Hence this frequency does not appear on the FRF of the rigid case. The second case study is designed to indicate how the properties of typical interface parameters, mainly stiffness, affect the response coupling results.
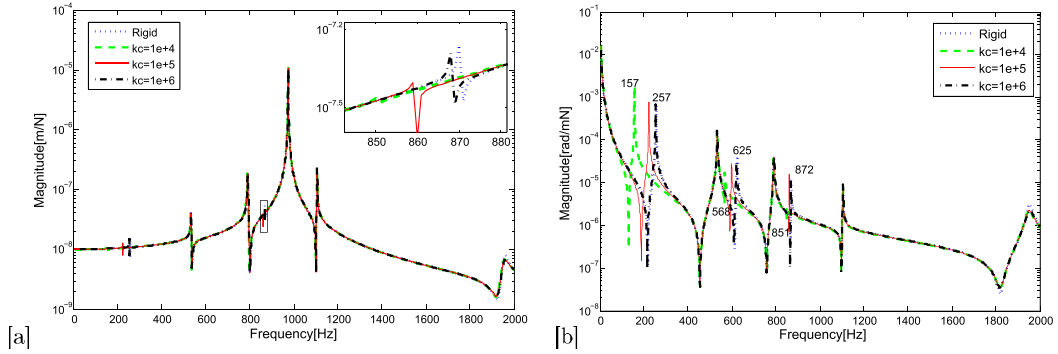
Figure 5. FRF (a) in the radial direction of the second bearing with flexible connector and (b) in the torsional direction.

4.3. *Effect of coupling stiffness*

The interest of interface between two subsystems is investigated for the coupling systems, it is of interest to understand their effects on system response (FRF). The term $D = (_A[\boldsymbol{H}]_{cc} + {}_B[\boldsymbol{H}]_{cc} + [\boldsymbol{K}]_s^{-1})$ present the relationships between the dynamic stiffness of coupling terms and the interface of the system behavior. The global system response indicates the significant contributions of these terms $_A[\boldsymbol{H}]_{cc}$, $_B[\boldsymbol{H}]_{cc}$, and $[\boldsymbol{K}]_s^{-1}$. Let $[H1(\omega)] = {}_A[\boldsymbol{H}]_{cc} + {}_B[\boldsymbol{H}]_{cc}$, and $[C(\omega)] = [\boldsymbol{K}]_s^{-1}$. Therefore, $[D] = ([H1] + [C])^{-1}$. $[H1(\omega)]$ illustrates the receptance properties of the two subsystems, whereas $[C(\omega)]$ corresponds to the receptance characteristics of the coupling. Hence, the impact of the subsystems and the connection parameters on system response is examined in this expression D. So, the following three cases were considered.

Case 1: $[H1] \ll |[C]|$. The dynamic stiffness at the points of subsystems coupling are higher than the connector stiffness.

The diminution in the assembled system response is due to the reduction in the coupling stiffness, as expected.

Case 2: $|[H1]| \approx |[C]|$. The coupling stiffness has the same order of magnitude as that of the connector stiffness, reduced $[K_s]$ still decreased the coupling system response. However, the effect of flexible coupling in case 1 is more significant than this case.

Case 3: $|[H1]| \gg |[C]|$. For important stiffness connectors, the assembled system response approaches to rigid connection system response [19].

In this case, it should be noted that the response of the system is close to the rigid system.

The same effect appears in the response of subsystem *B*. There is a difference in frequency and magnitude. As a result, the coupling dynamics cannot be neglected when examining dynamic responses. The results moreover displayed that the existence of the connection declined the natural frequencies and the magnitude as proved in [19, 27]. In addition, the coupling natural frequency is found to be quite sensitive to coupling stiffness. Nevertheless, the curves are superposed notably on the frequencies of the subsystem *A* with slight variation.

It can be noted that the rotational direction of the shaft is sensitive to shaft stiffness coupling. The results indicate that the presence of a flexible coupling shifts the frequencies lower. These frequencies in the rigid coupling case are identified at 257 Hz, 625 Hz and 872 Hz, whereas those in the elastic coupling case are located respectively at 157 Hz, 568 Hz and 851 Hz. For the second case, the latter are located at 224 Hz, 599 Hz and 860 Hz. While the frequencies of the third case are close to the rigid case. These frequencies are located at 253 Hz, 621 Hz and 868 Hz. Furthermore, the results prove that the appearance of the coupling participated
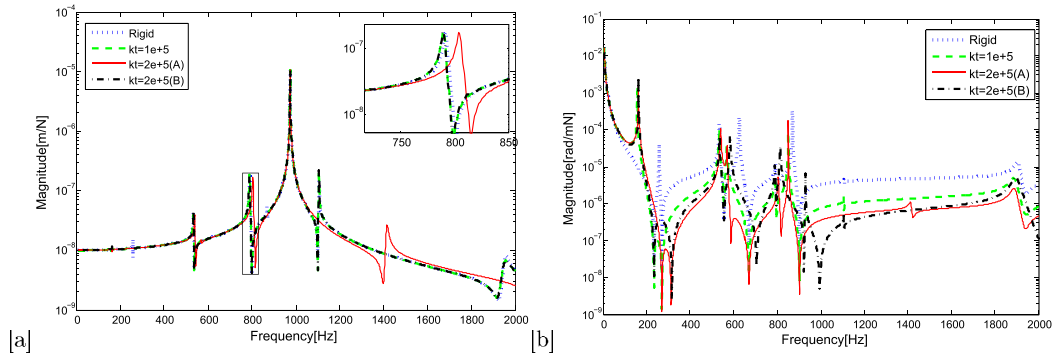
Figure 6. Effect of shaft stiffness on the FRF (a) radial direction (b) coupling direction.

in the lowering of frequencies which hinders the reduction of vibration due to coupling. These results were proved by Hmida, Han and Tadeo in [14, 27, 29]. In order to highlight the influence of subsystem parameters on coupled FRFs, numerical simulations are performed considering different dimensionless stiffness of bearings and shafts.

### 4.4. *Effect of shaft stiffness on flexible coupling method response*

A parametric study is conducted for the purpose of analyzing the effect of shaft stiffness variations of two subsystems *A* and *B* on the flexible coupling method response. In this research, $[K]_s$ is conserved but the free FRFs are modified to explore their influence on the joined system response.

The contributions of the shaft stiffness was indicated considerably on the global system response. Two distinct dimensionless shaft stiffness $kt = 1 \times 10^5$ and 2×10^5 of two subsystems were used to investigate their effect on global response. Figures 6(a) and (b) depict an FRF comparison employing two shaft stiffness in radial and coupling directions of subsystem A, respectively. Torsional and bending frequencies can be influenced by modification of intermediate shafts [30]. The coupling and subsystem *A* frequencies are influenced by the subsystem *A* shaft stiffness in the radial direction (shown in Figure 6(a)). In contrast, the variation of shaft stiffness of subsystem *B* affects only the coupling frequency. The assembled system response approaches the rigid connection system response due to increase in shaft stiffness of subsystem *B*. Additionally, shaft stiffness affects the coupling frequency in the case of torsional coupling. The frequency response around mode 4 is involved by reason of increasing the shaft stiffness of each subsystems, which is shown in the zoomed inset in Figure 6. Figure 6(b) shows the difference in magnitude in the case of flexible coupling especially when increasing the stiffness rigidity of subsystem *A*. Nevertheless, when the subsystem stiffness *B* is enhanced, no important modification in the system response spectrum is noticed.

The curves show that the vibratory level of the coupling frequencies appears significant in the coupling direction, while this level is lower in the radial direction.

4.5. *Effect of bearings stiffness on the coupled system FRF*

A parametric study is conducted to analyze the effect of bearing stiffness variations on the dynamic response. Figures 7(a,b) and 8 depict an FRF comparison using two different bearing stiffness values in radial, rotational, and coupling directions of subsystem *A*. It can be noted that
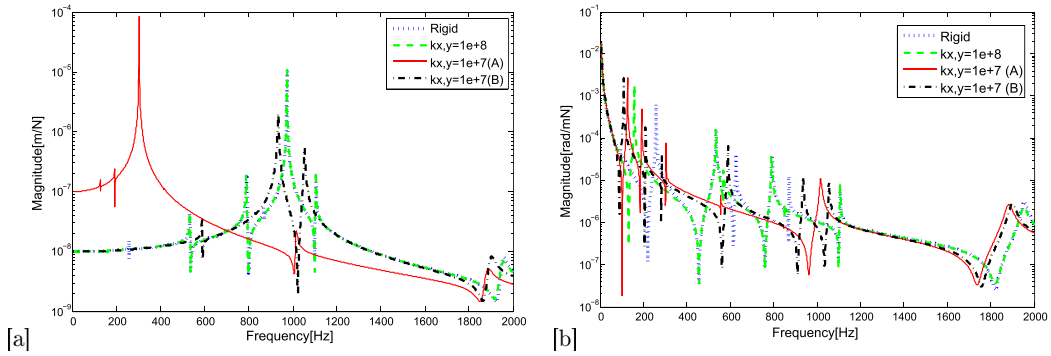
Figure 7. Effect of shaft bearing stiffness on the FRF (a) radial direction and (b) rotational direction.
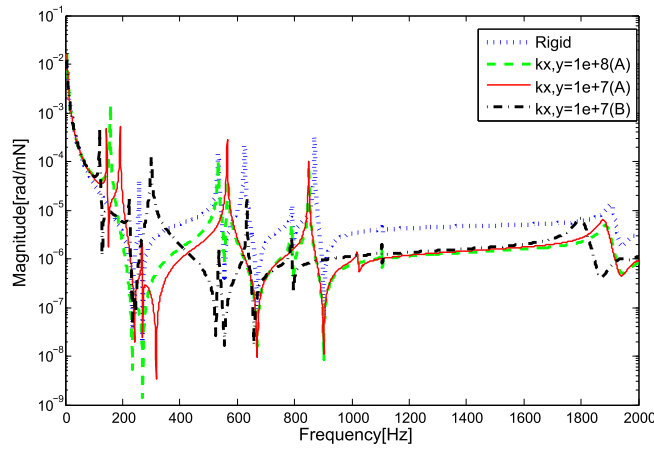
**Figure 8.** Effect of shaft bearing stiffness on the FRF coupling direction.

the dynamic response in the radial direction is more sensitive to bearing stiffness variation of subsystem *A*. This result is consistent with the research work of Wang [12] which showed that the variations in the main bearing stiffness exerts a weak influence on the dynamic response of the planet carrier but a stronger influence on the main shaft bearing stiffness. Therefore, it shows a difference in frequency and magnitude. In addition, an important difference in magnitude is observed. The stiffness bearing variation of subsystems *A* and *B* affected the coupled system frequency. Nonetheless, the bearing stiffness variation of subsystem *B* affects especially the coupling frequency on the FRFs coupled subsystem *A* (Figure 7(b)).

While the results in Figure 7 show that the coupled frequencies and the frequencies of the subsystem *A* are sensitive to the bearings' rigidity variation of subsystem *B*.

The coupling frequency is insensitive to the bearing stiffness variation of subsystem *B* in the case of torsional coupling direction (show Figure 8). It is clear that the bearing stiffness does not affect the coupling frequency in the torsional direction.

4.6. *Effect of translational and torsional coupling stiffness on the coupled system FRF*

It is of interest to investigate the effect of translational and torsional coupling on system response. Equation (13) was used, where the term $B = {}_AH_{cc} + {}_BH_{cc} + [H_j]$ presents the relationships between
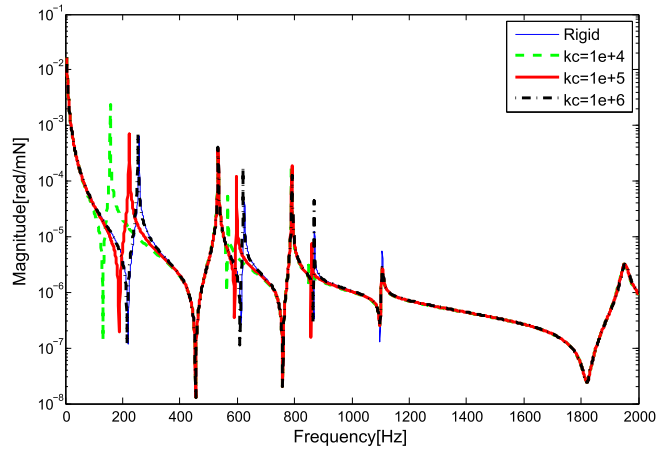
Figure 9. FRF in torsional direction of the second shaft with the second Nelson's model.

the dynamic stiffness of coupling terms and the interface of the system behavior. The elastic coupling is approached via a Nelson second model where translational parameters are (k_{xc}, k_{yc}),(c_{xc}, c_{yc}) and torsional parameters are ($k_{\theta c}$), ($c_{\theta c}$). The classical receptance method is not valid, so the formulation of the RC is different from the standard approach. In this case, the second RC method was used.

Figure 9 depicts the FRF of a subsystem A with a rigid and a flexible coupling in the torsional direction of the second shaft. The results show a decrease in the coupling natural frequencies due to the existence of the connector. For the different directions, it shows the difference among the natural frequencies expected by the rigid and the flexible coupling of the Nelson and Crandall second model. In other directions, the models of joints have the same effect between two flexible coupling models. The models of joints affect the coupling direction FRF.

### 4.6.1. *Investigation of the effect of torsional coupling stiffness*

To discover the influence of torsional coupling stiffness on system response, gear systems with variable coupling stiffness are implemented. So, the effect of torsional FRF of joint on system response is outlined in Figure 9. The reduction in the assembled system response is due to the coupling stiffness. Additionally torsional coupling stiffness is sensitive to the natural frequency of coupling. For important values of stiffness interface, the assembled system response approaches the rigid connection system response for all directions.

4.6.2. *Investigation of the effect of translational coupling stiffness*

The characteristics of the mechanical joint affect a system's responses. Figures 10(a) and (b) indicate the effect of translational coupling stiffness on system response. Three different dimensionless translational coupling stiffness were taken: $kxa = kya = 462 \times 10^2$ N/m, 462×10^5 N/m and 462×10^7 N/m. Figure 10(a) shows the effect of the parametric study of the translational stiffness in the linear direction. By comparing the two cases of coupling, the results show that the translational stiffness coupling does not affect these FRFs due to the higher value of bearing stiffness. The translational coupling stiffness affects slightly the eigen-frequencies of subsystem A. Increased translational coupling stiffness leads to an increase in the frequencies of subsystem A. Nevertheless, the response in torsional direction is not influenced by the variation of translational coupling stiffness (show Figure 10(b)). System response is sensitive to translational
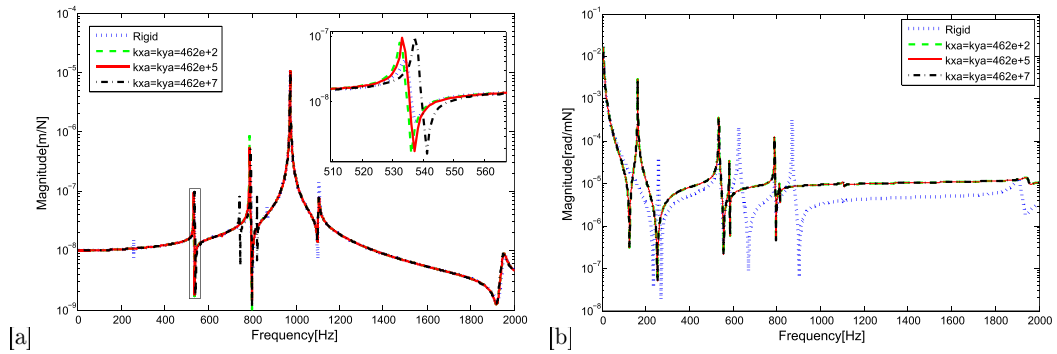
Figure 10. FRF with the second model of Nelson (a) in the linear direction of the second bearing and (b) in the torsional direction of the second shaft.
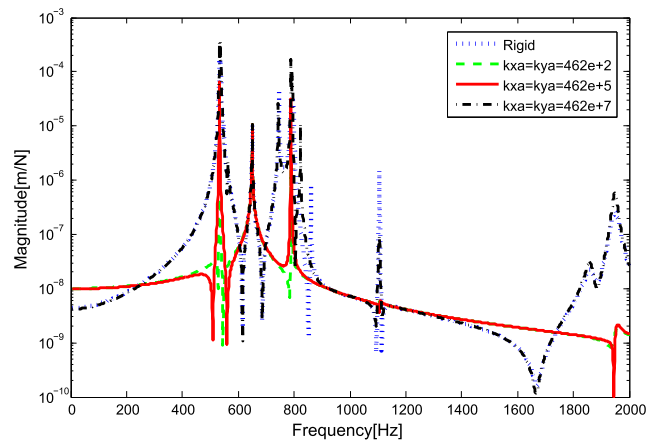
Figure 11. FRF in the translational coupling direction.

coupling stiffness in coupling DoF (show Figure 11). For a high value of translational stiffness coupling, it shows in Figure 11 that the response approaches the rigid connection system response.

It can be concluded that the torsional coupling stiffness variation is more sensitive than the translational coupling stiffness.

5. Conclusions

This manuscript discussed the impact of different models and characteristics of elastic coupling on the dynamic behavior of the system. In this paper, one of the important techniques of the substructuring method—the receptance method—is used for the transmission system. The studied system is a reducer stage connected by two models of coupling a rigid and a flexible coupling. The aforementioned technique is proposed to predict their behavior dynamics by using FRFs of subsystems. The effects of the main shaft bearing stiffness and elastic interface stiffness on the FRF were investigated. In addition, the parameters of coupling models for which we adopt the second model of Kramer and the second model of Nelson and Crandall were developed to investigate the dynamic response of the studied system.

The conclusions obtained are listed as follows:

(1) The results achieved are compared with those of Hmida [27] and a great correspondence of natural frequencies is noted. By calculating the FRF obtained by the rigid coupling and those coupled by flexible coupling, different results have been obtained in the frequencies. In fact, it is noticed that the coupling natural frequencies were reduced through the use of an elastic coupling and moreover the FRF amplitude. It can be noted that the rotational direction of the shaft is sensitive to shaft stiffness coupling.

(2) Variation of shaft stiffness of subsystem *A* has considerable influence on the coupling frequency in the radial direction. Nevertheless, when the subsystem stiffness *B* is enhanced, no important modification in the system response spectrum is noticed. Thus, the change of shaft stiffness of subsystem *B* exerts a weaker influence on the coupling frequency.

(3) The dynamic response of subsystem *A* is more sensitive to variation bearing stiffness of subsystem *A* but a weaker sensibility to variation of subsystem *B* especially in the radial direction.

(4) The impact of translational stiffness coupling on the RC method is investigated. It was reported that the torsional coupling stiffness is more sensitive than the translational coupling stiffness. Thus, the translational coupling stiffness has not affected the response of subsystem in the rotational direction.

Nomenclature

Ks	Stationary stiffness matrix of bearing and shaft
$[C(\omega)]$	Receptance characteristics of the coupling
$[H1(\omega)]$	Receptance characteristics of the two subsystems
h_{tt}	Receptance matrix of the joint according to translation direction
h_{rr}	Receptance matrix of the joint according to rotation direction
$n[x]i$ and $n[\theta]i$	Translational and rotational displacement vectors
$[H_j]$	Receptance matrix of the joint
$K(t)$	Time-varying mesh stiffness matrix
$[km]$, $[cm]$	The gear mesh stiffness and damping
$k_{\theta c}$	Torsional stiffness
$_A[\boldsymbol{x}]_i$, $_A[\boldsymbol{\theta}]_i$	Translational and rotational displacement vectors
$Hjk(\omega)$	The steady-state displacement at coordinate j due to a harmonic force excitation at coordinate k
$c_{\theta c}$	Torsional damping
$r_{\boldsymbol{\Phi}j}$	Mass-normalized eigen-vector
FRF	Frequency response function
TDOF	Translational degree of freedom
RDOF	Rotational degree of freedom
RC	Receptance coupling
C	coupling DoFs
FBS	Frequency-based substructuring

Conflicts of interest

Authors have no conflict of interest to declare.

References

[1] H. Jalali, H. Ahmadian, "Identification of bolted lap joints parameters in assembled structures", *Mech. Syst. Signal Process.* **21** (2007), no. 2, p. 1041-1050.

[2] H. N. Ozguven, E. Budak, O. Ozashin, A. Erturk, "A closed form approach for identification of dynamical contact parameters in spindle-holder-tool assemblies", *Int. J. Mach. Tools Manuf.* **49** (2009), no. 1, p. 25-35.

[3] M. R. Movahhedy, S. S. Park, Y. Altintas, "Receptance coupling for end mills", *Int. J. Mach. Tools Manuf.* **43** (2003), no. 9, p. 889-896.

[4] C. Brecher, P. Chavan, "Efficient joint identification and fluted segment modeling of shrink-fit tool assemblies by updating extended tool models", *Mach. Tool* **15** (2021), p. 21-33.

[5] C. F. Beards, Y. Ren, "Identification of effective linear joints using coupling and joint identification techniques", *J. Sound Vib.* **120** (1998), p. 331-338.

[6] D. J. Ewins, W. Liu, "Substructure synthesis via elastic media. Part I: joint identification", in *IMACXVIII: A Conference on Structural Dynamics*, San Antonio, TX, 2000.

[7] W. Liu, "Structural dynamic analysis and testing of coupled structures", PhD Thesis, University of London, Imperial College of Science, Technology and Medicine, 2000.

[8] J. Chae, S. S. Park, "Joint identification of modular tools using a novel receptance coupling method", *Int. J. Adv. Manuf. Technol.* **35** (2008), p. 1251-1262.

[9] R. Pettit, A. Ibrahim, "Uncertainties and dynamic problems of bolted joints and other fasteners", *J. Sound Vib.* **279** (2005), p. 857-936.

[10] A. E. Mahmoudi, D. J. Rixen, C. H. Meyer, "Comparison of different approaches to include connection elements into frequency-based substructuring", *Exp. Tech.* **44** (2020), no. 4, p. 425-433.

[11] S. Tsai, H. Ouyang, J. Chang, "A receptance-based method for frequency assignment via coupling of subsystems", *J. Exp. Tech.* **90** (2020), no. 44, p. 425-433.

[12] S. Wang, C. Zhu, C. Song, H. Han, "Effects of elastic support on the dynamic behaviors of the wind turbine drive train", *Front. Mech.* **12** (2017), no. 3, p. 348-356.

[13] M. Mataar, T. Fakhfakh, M. Haddar, S. Bouaziz, M. A. Hili, "Dynamic behavior of hydrodynamic journal bearings in presence of rotor spatial angular misalignment", *Mech. Mach. Theory* **44** (2009), no. 8, p. 1548-1559.

[14] K. L. Cavalca, A. T. Tadeo, "A comparison of flexible coupling models for updating in rotating machinery response", *J. Braz. Soc. Mech. Sci. Eng.* **25** (2003), no. 3, p. 235-246.

[15] E. Kramer, *Dynamics of Rotors and Foundations*, Springer-Verlag, New York, 1993.

[16] S. H. Crandall, H. D. Nelson, "Analytic prediction of rotor dynamic response", in *Handbook of Rotordynamics* (F. E. Ehrich, ed.), McGraw-Hill Inc, New York, 1992.

[17] M. Mariunas, V. Chaika, "Dynamic behavior of a harmonically excited electromechanical drive with elastic couplings", *J. Vib. Acoust.* **119** (1997), no. 1, p. 21-30.

[18] M. Chouksey, A. Saxena, A. Parey, "Study of modal characteristics of a geared rotor system", *Proc. Technol.* **23** (2016), p. 225-231.

[19] J. Zhen, T. C. Lim, G. Lu, "Determination of system vibratory response characteristics applying a spectral-based inverse sub-structuring approach. Part I: analytical formulation", *Int. J. Veh. Noise Vib.* **1** (2004), p. 1-30.

[20] M. Bouslema, A. Frikha, M. Abdennadar, T. Fakhfakh, R. Nasri, M. Haddar, "Effects of modal truncation and condensation methods on the Frequency Response Function of a stage reducer connected by rigid coupling to a planetary gear system", *C. R. Mec.* **345** (2017), p. 807-823.

[21] B. Jetmundsen, R. Bielawa, W. G. Flannelly, "Generalized frequency domain substructure synthesis", *J. Am. Helicopter Soc.* **33** (1988), no. 1, p. 55-64.

[22] B. L. Choi, J. M. Park, "Application of the impedance coupling method and the equivalent rotor model in rotordynamics", *J. Finite Elem. Anal. Des.* **39** (2002), no. 2, p. 93-106.

[23] K. Cuppens, P. Sas, L. Hermans, "Evaluation of the FRF based substructuring and modal synthesis technique applied to vehicle fe data", in *Proceedings of ISMA*, Leuven, 2003.

[24] P. Sjovall, T. Abrahamssoon, "Substructure system identification from coupled system test data", *Mech. Syst. Signal Process.* **22** (2008), no. 1, p. 15-33.

[25] L. Walha, "Contribution A la Dynamique Non Lineaire Des Reducteurs A Engrenages (Prise en compte des jeux fonctionnels et du frottement entre dentures)", PhD Thesis, University of Sfax, Ecole Nationale D'ingénieur de Sfax, 2008.

[26] F. Chaari, W. Baccar, M. S. Abbes, M. Haddar, "Effect of spalling or tooth breakage on gearmesh stiffness and dynamic response of a one-stage spur gear transmission", *Eur. J. Mech. A/Solids* **27** (2008), p. 691-705.

[27] A. Hmida, A. Hammemi, T. Khbou, F. Chaari, M. Haddar, "Effect of elastic coupling on the modal characteristics of spur gearbox system", *Appl. Acoust.* **144** (2019), p. 71-84.

[28] M. Bouslema, A. Frikha, T. Fakhfakh, R. Nasri, M. Haddar, "FRF of a coupled geared system using the frequency based substructuring and condensation methods", *Proc. Inst. Mech. Eng. D: J. Automob. Eng.* **10** (2022), p. 1-18.

[29] H. HyungSuk, L. KyoungHyun, P. SungHo, "Evaluation of the increased stiffness for the elastic coupling under the dynamic loading conditions in a ship", *Eng. Fail. Anal.* **68** (2016), p. 254-262.

[30] H. Lorenzen, E. A. Niedermann, W. Wattinger, "Solid couplings with flexible intermediate shafts for high speed turbo compressor trains", in *Proceeding of the 18th Turbomachinery Symposium*, Texas, 1989, p. 101-110.